

Article

Not peer-reviewed version

---

# Hailstorms That Produce Very Large Hail: Which Are the Differences with Other Thunderstorms?

---

[Tomeu Rigo](#)\*

Posted Date: 9 March 2026

doi: 10.20944/preprints202603.0593.v1

Keywords: hail; large stones; thunderstorms; weather radar; vertical profile of reflectivity; VIL density; echotop



Preprints.org is a free multidisciplinary platform providing preprint service that is dedicated to making early versions of research outputs permanently available and citable. Preprints posted at Preprints.org appear in Web of Science, Crossref, Google Scholar, Scilit, Europe PMC.

Copyright: This open access article is published under a [Creative Commons CC BY 4.0 license](#), which permit the free download, distribution, and reuse, provided that the author and preprint are cited in any reuse.

Disclaimer/Publisher's Note: The statements, opinions, and data contained in all publications are solely those of the individual author(s) and contributor(s) and not of MDPI and/or the editor(s). MDPI and/or the editor(s) disclaim responsibility for any injury to people or property resulting from any ideas, methods, instructions, or products referred to in the content.

Article

# Hailstorms That Produce Very Large Hail: Which Are the Differences with Other Thunderstorms?

Tomeu Rigo

Forecast Area, Servei Meteorologic de Catalunya, Barcelona, Dr. Roux, 80, 08013; tomeu.rigo@gencat.cat

## Abstract

Hail events commonly affect the Western part of Catalonia, producing important damages mainly in Agriculture sector. The comparison of the weather radar data with the hail-pad registers at ground level allows to improve the diagnosis of hail in thunderstorms and to estimate the maximum hail size. However, there are some limitations using individual radar fields (such as the maximum reflectivity, the echo top or the density of the vertically integrated liquid). The current research has been conducted using quantiles of the vertical profiles of reflectivity for different times before, during and after the hailfall. First, it has been shown that these profiles relate to all the radar parameters. Second, it has been demonstrated that are less sensitive to anomalies of the radar functioning. The final purpose of the project is to develop a real-time tool that improves the surveillance task to discriminate between non-hail and hail thunderstorms and severe and non-severe hail occurrence.

**Keywords:** hail; large stones; thunderstorms; weather radar; vertical profile of reflectivity; VIL density; echotop

---

## 1. Introduction

According to [1], hail is any regular or irregular ice particle falling from a thunderstorm with a diameter exceeding 5 mm. It is one of the most damaging phenomena in different regions around the World, such as the United States of America (USA) [2], Canada [3], Argentina [4], Europe [5], China [6], or Australia [7], among others. Based on [8], hail damages are increasing in recent years and are comparable in annual losses to hurricanes in the USA. Agriculture is the sector most affected by hailstorms, but not the unique, with several cases of important damages to buildings, cars, infrastructures and even people, with events producing injuries and even some casualties [9–12]. Even large hail producing thunderstorms have big dimensions and very intense updrafts [1,13,14], it is still a challenge their mid-term forecasting (between one and two days in advance) and hail size diagnosing [15–17]. The main cause is the difficulty of reproducing the large number of internal processes occurring inside the thunderstorms [18], which includes electrification [19], wet and dry growth and riming of hailstones [20–23], and very strong updrafts and other thermo-dynamic physics [24].

[9,10,25] showed the high relationship between the hailstones size and the effects at ground, generally using weather radar information and comparing with direct observations. One of the usual issues of this type of Research is the high dependance of observations with the population density. Other studies have compared the radar fields with economic losses, most of times provided by insurance [26,27]. However, this source is not always easy to acquire, because of the politics of privacy of these companies. Size and shape, among other atmospheric factors, help to increase the terminal fall speed of the stones, increasing the impact on the hit surface [28]. [29] show that hail-pads (plastic foils that change the surface properties when they are hit by stones) are very useful for measuring this impact in real situations.

The previous paragraphs presented the importance of weather radar and hail pads to diagnose hail inside a thunderstorm and estimate the hail size distribution precipitated by the same storm [30,31]. The two systems are highly valuable to understand the hailstorm evolution. Hail pad

networks [32] provide very useful data in large areas (ranging between 100 and 1,000 km<sup>2</sup>) with a high spatial resolution, this is, a short distance between pads. Each hail pad provides the distribution of stones giving information about the size and the energy of impact. The disadvantage is that this information is acquired with delays with respect to the event occurrence (usually, more than one day, and the final processed data with more than six months) [30]. Therefore, it is not useful for real time surveillance tasks. In contrast, weather radar fields provide volumetric information inside the thunderstorm that allows us to infer the dynamic behavior of the cloud [17]. However, ground surface hail size estimation is not always accurate, because different system limitations [33]. The comparison of both sources, which is made when hail-pad data is available, helps to calibrate the different radar parameters and provide more precise maps of hail size occurrence and distribution [25].

The limitation of the weather radar to provide realistic estimations of hail size at ground level [1] has led to the development of different radar products and the identification of signatures that have helped in the diagnosis of the phenomenon at different levels, depending on the system technology and the product characteristics. There are a wide range of products, with diverse degrees of complexity, depending on the level of process. Here we summarize most of them, but only introducing the relevant information, because the objective of the manuscript isn't analyzing all of them. The analysis of Ortega [34] evaluating multiple radar products in a project comparing those fields with ground observations in the United States is one of the best guides to identify the most common fields. The included products are: Maximum Expected Size of Hail (MESH), Probability of Severe Hail (POSH), the echo tops for the 50 and 60 dBZ thresholds (or the maximum height where echoes exceed those thresholds in a radar column), the Vertically Integrated Liquid (VIL, or the integration of the reflectivity at all vertical levels of a radar column) and VIL density (this is, the VIL divided by the echo top), the ground reflectivity, the Vertically Integrated Ice (VII, similar to VIL, but only for the echoes between heights with temperature between -10 and -40 °C), and the maximum reflectivity. The most significant result was that the products better correlated with hail were those that considered the vertical development of the thunderstorm. Ciță et al. [35] did a similar Research in Romania, but using less products: composite reflectivity at low levels, VIL, Echo Top, Vil density, and the Hail Kinetic Energy (HKE), a product estimated like the VIL, but more oriented to be compared with hail-pad observations because it uses an empirical equation calculated from the relationship with previous observations. HKE and VIL density provided the best evaluating indices, which were very similar in both cases. The VIL is one of the most common products and [36] made a comparison with different versions of this field with different configurations, based on heights of different temperature thresholds associated with the hail formation in Poland. They estimated VIL between different layers, the reflectivity field at 8 km, and the Probability of Hail (POH) based on the difference between the echo top and the freezing height. In this study best agreements of the ground register coincide with the last parameter. There are other variables obtained from dual polarization [37], which theoretically provides better results than single polarization. However, because the present study has been made using single-pol weather radar, it is not necessary to go in deep with these polarimetric fields. Finally, [1] summarizes some signatures observed in radar fields that can be associated with hail occurrence, because the interaction of the beam with the stones (TBSS, Three-Body Scattering Signature), or the region (BWE, Bounded Weak Echo) with null reflectivity values caused by the strong updrafts in hailstorms. However, it is very difficult to relate these signatures with exact sizes at ground level.

Hail in Catalonia occurs recursively each year, with a high variability respect on the number of cases, the maximum size occurred, the monthly distribution, or the spatial distribution along the territory during a year [38]. Aran et al. [39] showed how a favorable synoptic configuration is the basis for hail occurrence, but it is not a definitive condition. The properties of the stones are also variable depending on the season [40–42], with a clear dependence on the thermodynamic conditions. The region has suffered notable hail events, some of them reported in [12] or [43]. The Servei Meteorològic de Catalunya (SMC) put in operational the first version of the Lightning Jump

algorithm (a signature of a sudden rise of total lightning in a thunderstorm, associated with the strong updraft and the production of hail) in 2020 [44]. Because of the high impact on agriculture [45], there is an operational hail pad network in the Western region to analyze the events that produce large damages in different kinds of agricultural exploitations [30,41]. [46] made a first analysis using the life cycle of thunderstorms to see the evolution of different radar parameters (Echo top, VIL, and reflectivity), indicating that as faster grew thunderstorms, higher was the probability of hail occurrence at ground.

Bearing in mind the recent events with hail sizes exceeding 10 cm (the largest size that the SMC has notice in the area ever) and that some of those thunderstorms had dimensions never observed before in the region (with like-tropical dimensions), and using weather radar and hail pad data, the principal question that this Research tries to answer is if there any relationship between the thunderstorm dimensions and the hail observed at ground. To do this, it has considered all impacted hail-pads from the period 2016-2025 and it has evaluated the evolution of different radar parameters (VIL density, reflectivity and echo top) over the ground location for a 24-minute interval.

## 2. Area of Study, Data and Methodology

### 2.1. Area of Study

The area of study includes a flat region at the Western of Catalonia (NE of the Iberian Peninsula, black rectangle in panel A of Figure 1), with a total size of 4,240 km<sup>2</sup> (yellow region in panel B of Figure 1). The region has been selected because it has a hail-pad network with available data since 2001 [41]. Furthermore, the region has enlarged with a buffered section (red area in the same figure), to include radar information for all the selected events. Therefore, the total size of the study region is 7,200 km<sup>2</sup>. The area of study is well-known for the high impact of hailstorms in its agricultural industry, with irrigated and rainfed crops depending on the water management [30,32,39,41,43,45,46]. In this case, it has been selected because ground hail observations (from the hail-pads) and volumetric weather data (panel C of Figure 1) are both available for a long period of time (in this case, the 10 years from 2016 to 2025).

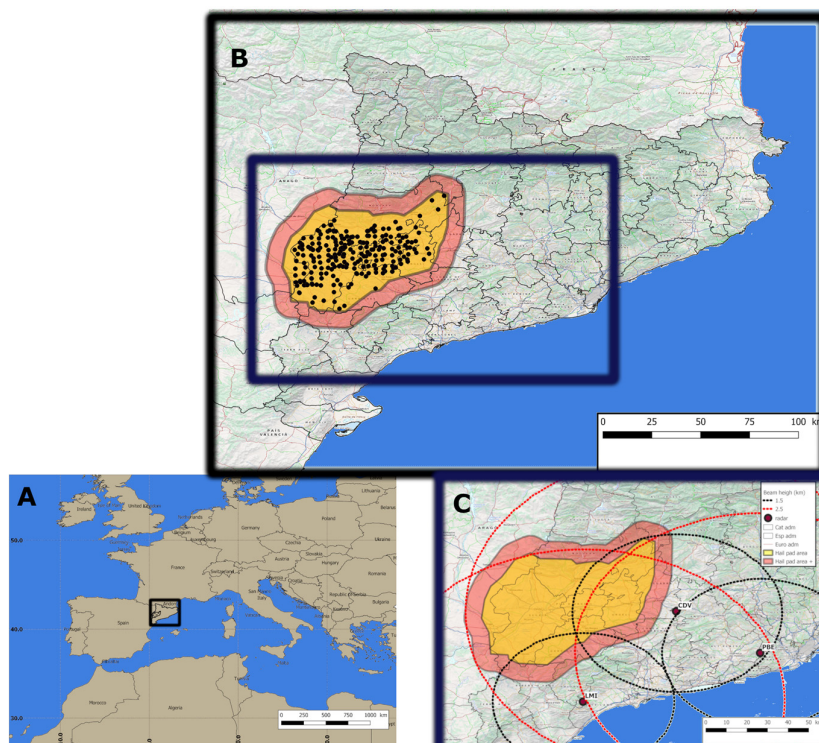


**Figure 1.** A: European map with Catalonia inside a black rectangle. B: Zoom to Catalonia with the region of interest in a blue rectangle. Black dots correspond to the hail-pads and the yellow area to the zone covered by the hail campaigns. The red area is a buffered region to include information from radar data. C: Zoom to the region of study and to the three of the four radars of the SMC network (red dots). Black and red dashed lines indicate the beam height of 2.5 and 3.5 km.

## 2.2. Data

The preliminary data source for the selection of the events comes from the records of each hail-pad of the network shown in panel B of Figure 1. The network consists of more than 150 elements (depending on the campaign) which are distributed in a semi-regular grid with 4 km between each sensor. This high resolution allows having a very good distribution of the hailfalls occurred in the region. In the present study the unique considered data is the maximum hail size, but other characteristics are measured (mean size, kinetic energy, density, among others). It is managed by the ADV-Terres de Ponent organization, in collaboration with the SMC and the University of Leon.

Weather radar data is of the XRAD (Radar network of the SMC). Panel C of Figure 1 shows how the area is well covered by three radars (lowest beam height below 2.5 km -red dashed lines- for two of them and the third not exceeding the 3.5 km, which is a height that allows characterizing adequately the thunderstorms in three dimensions [42]). The products have a time resolution of 6 minutes and are a composition of the maximum value at each point. The used fields are the volumetric reflectivity, with a grid size of 2x2x1 km, with CAPPI (Constant Altitude Plan Position Indicator) heights between 1 and 10 km. Besides, the TOP45 (or maximum echo top for a reflectivity threshold of 45 dBZ) and the VIL density are used for comparing with each ground observation (both products with grid size of 1x1km).

## 2.3. Methodology

Figure 2 shows the scheme of the methodology considered in the Research. For each hail-pad register (which includes the date, longitude, latitude, and the maximum diameter of the stone) it has been searched for the time with the highest maximum reflectivity value over the hail-pad coordinates in the 6-minute volumetric radar composite. The time of the highest maximum reflectivity is defined as the time of the hailfall. The next step is to calculate the maximum reflectivity (equivalent to the intensity of the thunderstorm), the VIL density (the measure of the water content in the cloud) and the TOP45 (the vertical development of the more intense nucleus of the thunderstorm) for the period between 12 minutes before and 12 minutes after the time of the hailfall, with 6 minutes gap. The 6-minute values of each variable have been estimated for a radius of 5 km to have a more accurate measurement of the thunderstorm dimensions. The next step of the process is the comparison of those parameters for the two types of hail registers, non-severe (below 2 cm of diameter) and severe, for 1,086 registers between 2016 and 2025. Finally, these results are compared with the vertical profiles of reflectivity for the area surrounding the hail-pad, to identify the pattern associated with each type of hailstone size.

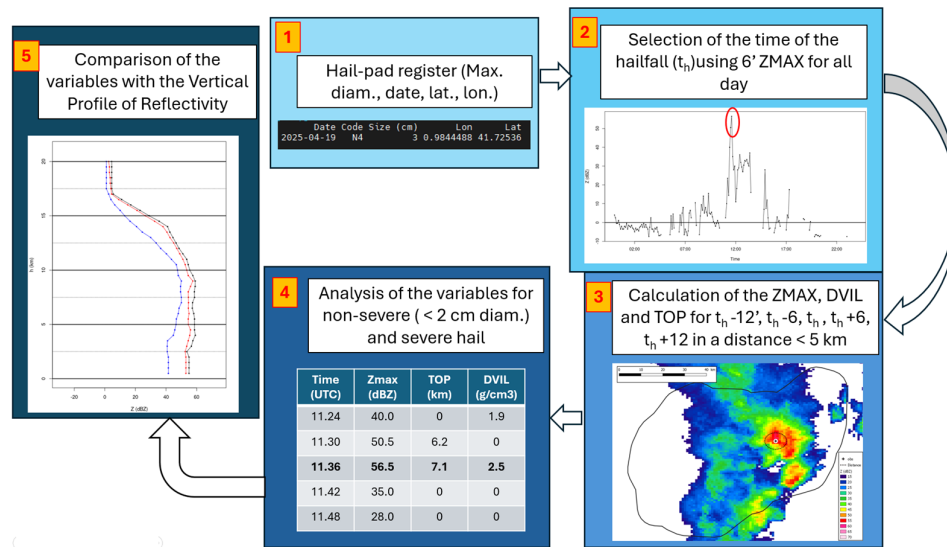


**Figure 2.** Scheme of the methodology: (1) selection of the hail-pads with hailfall registers for the period 2016-2025. (2) Identification of the time of the hailfall using 6-minute reflectivity information. (3) Estimation of the radar variables in a section of 5 km surrounding the hail-pad. (4) Analysis of the different variables for non-severe and severe events. (5) Comparison of the variables with the vertical profile of reflectivity.

### 3. Results

#### 3.1. Selection of the Events

The dataset consists of 1,443 registers of hail distributed in 120 events and proceeding from 174 different hail-pads. Data is collected only between April to September (exceptionally some October events were available). The period of analysis comprises the years 2016 to 2025 (sixty months in total). The most hit hail-pad registered 20 cases (indicating that the pad was hit in 1.1% of the days), with a mean value of 6.2 hail events per plaque. The event with a larger number of hit hail-pads was 19 April 2025 (60), while the mean value is 9.1 plaques per event. 6 days registered hail in 40 or more hail-pads (28 May 2016 -54-, 11 May 2017 -44-, 27 June 2017 -41-, 29 April 2018 -53-, 20 July 2018 -55-, 19 April 2025 -60-). These values are examples of the irregularity of the hailfalls in the region, in terms of number of hail-pads (extension of the event) and of the seasonality.

#### 3.2. Categorization of the Observations

Moving to the types of observations (non-severe and severe), there is high difference between both in the case of the number of registers and how they are distributed along the area of interest. Figure 3 presents all the cases (merging severe and non-severe) and shows how there are a major number of events per pad in the Western and Northern part. On the other hand, Southern and Eastern regions have a smaller number of hail events.

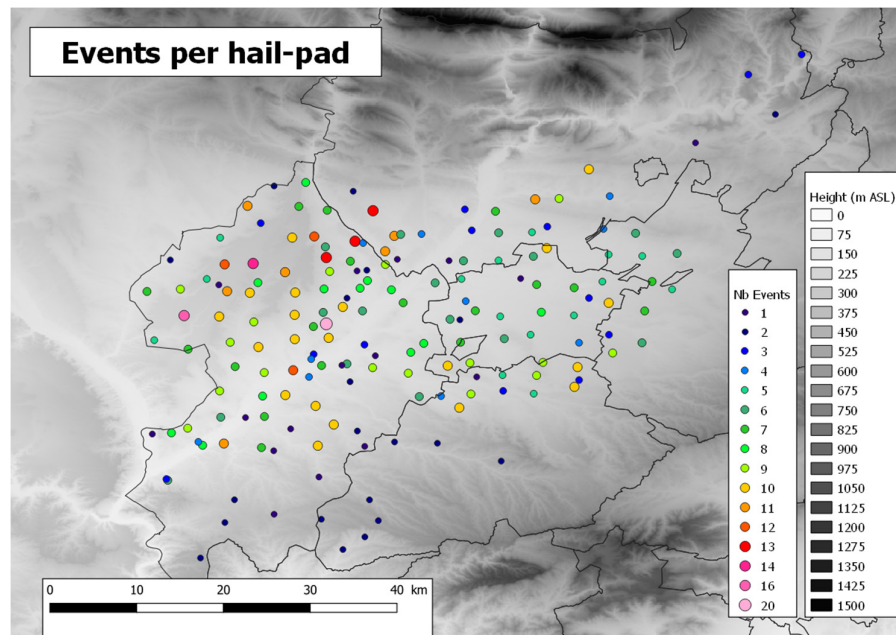


**Figure 3.** Number of hailfall days (events) for each sensor analyzed during the period 2016-2025 (the hail campaign goes from April to September yearly).

In the case of the two categories (Figure 4), non-severe hail events (panel A) have a similar configuration than the general one, indicating that most cases are of this type and, besides, that affect the same regions. However, severe events (panel B), which are less frequent, are also common (2 events) in the North-Eastern region. Furthermore, the Central and Southern areas present clear minima, and severe registers are infrequent or even null in some parts of those regions.

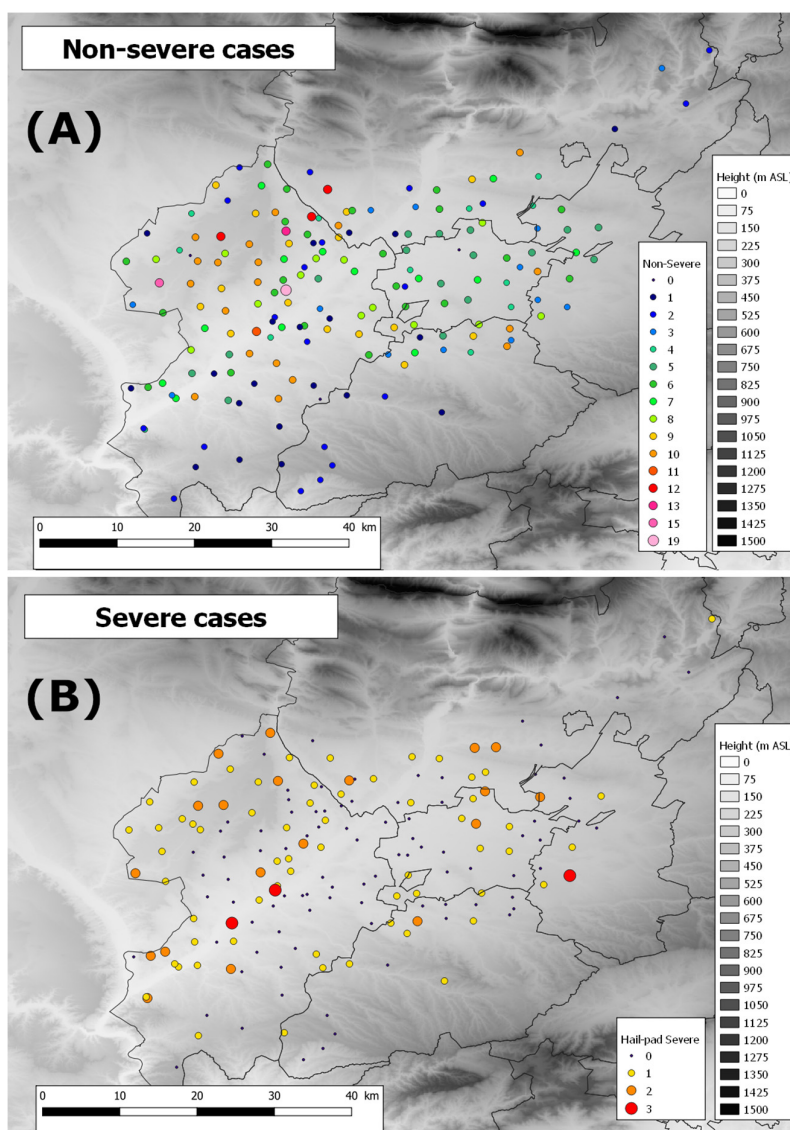


**Figure 4.** (A) Same as Figure 3 but for non-severe hail cases. (B) Same as Figure 3 but for severe hail cases.

### 3.3. Weather Radar Variables: Discrimination Between Hail Sizes

The purpose of this Research is to find differences in the behavior of the radar variables corresponding to the period of the hailfall over the hail-pad (from 12 minutes prior to the maximum reflectivity over the point to the 12 minutes later). Each one of the three radar variables represents a different characteristic of the hailstorm. The first one, the maximum reflectivity is equivalent to the intensity of precipitation associated with the thunderstorm. Figure 5 shows the differences between non-severe (left) and severe (right) cases. First, it is important to consider that both sets are different in number of cases: non-severe registers are more frequent (978 in front of 108 severe observations). In any case, it can be deduced the following points from the image: first, severe cases distribution is more compact, with less dispersion. In the same way, there are no outliers in the lower limit, as happens with non-severe distribution. Lastly, the value for the five moments are always higher in the case of severe hailfalls, with a mean value of 58 dBZ in front of the 55 dBZ for non-severe cases. If we pay attention in the time when the maximum occurs during the selected period (Table 1), the distribution is very similar for both categories, with a peak at the time of the hailfall, and some residual cases with the maximum prior to the hailfall. In any case, the maximum reflectivity occurred after the instant zero.

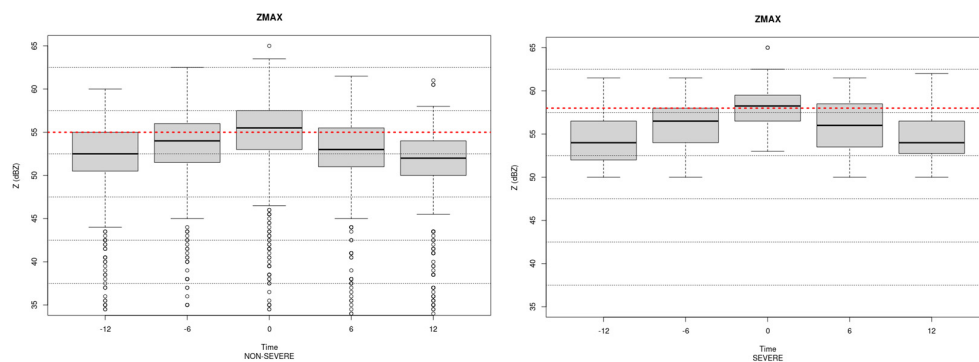


**Figure 5.** Boxplots for the maximum reflectivity for the 6-minute times for the period that goes from 12 minutes before to 12 minutes after the hailfall (the center indicates the time of the event). Left panel for all non-severe hail events and right panel for severe hail cases (2016-2025).

In the case of the Echo top (of 45 dBZ), which is the indicative of the vertical development of the more intense nucleus inside the hailstorm, the differences are also evident between non-severe and severe cases (Figure 6). In the first case, the boxes are more similar at all moments, with a slight increase until the hailfall, followed by a subtle decrease after that time. In the case of severe registers, the Echo top has more differences between all the boxes, indicating that the core reached the maximum development at the time of the hail occurrence. Besides, the values are in all moments between 1 and 2 km higher than in the case of non-severe events. In the same line, the mean value is 2 km higher for severe events (10 km in front of 8 km). A different behavior respect on the maximum reflectivity is found in the occurrence of the maximum value (Table 1). While the non-severe cases have again the maximum Echo top occurring during the zero moment, in the case of the severe events this maximum is displaced to the next radar image (6' later the hailfall). Another difference with reflectivity is that the distribution is more regular, with a higher percentage in all the moments different to the hailfall time.

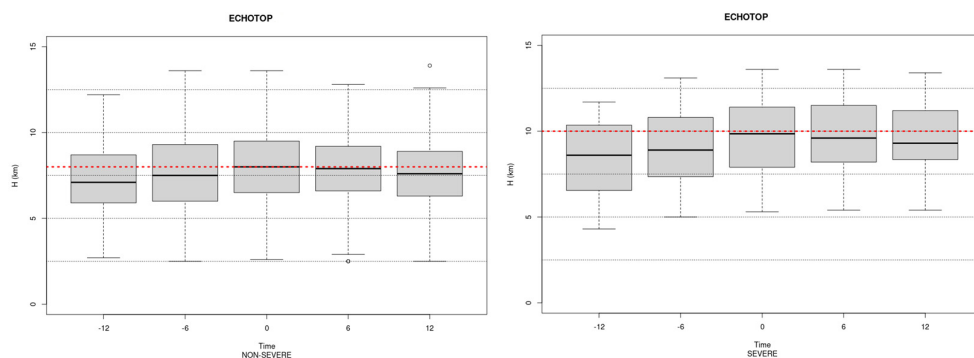


**Figure 6.** Same as Figure 5, but for Echo top (TOP45).

Lastly, VIL density (a measure of the water quantity inside the cloud) has a similar behavior than maximum reflectivity (Figure 7), but with wider boxes (larger dispersion of the data set respecting the mean value). In any case, the severe cases have in mean  $1 \text{ g/m}^3$  more of VIL density than non-severe cases. In this case, the distributions present sharp increases and decreases during the period with a clear peak at the hailfall time. Table 1 shows that more than 50% of the hailfalls had the maximum value of VIL density at the zero moment, for both categories.

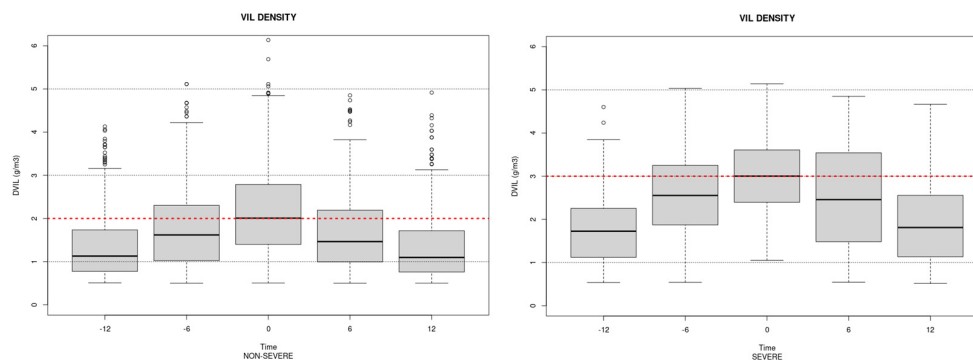


**Figure 7.** Same as Figure 5, but for VIL density (DVIL).

**Table 1.** Number of cases (the percentage in the parentheses on the right) that the maximum occurred at each time.

| Time | ZMAX (NSv) | ZMAX (Sev) | TOP (NSv) | TOP (Sev) | DVIL (NSv) | DVIL (Sev) |
|------|------------|------------|-----------|-----------|------------|------------|
| -12  | 18(2)      | 3(3)       | 66(7)     | 9(8)      | 48(5)      | 9(8)       |
| -6   | 91(10)     | 10(9)      | 135(14)   | 15(14)    | 157(17)    | 16(15)     |
| 0    | 847(88)    | 95(88)     | 341(36)   | 31(29)    | 526(56)    | 55(51)     |
| 6    | 0(0)       | 0(0)       | 288(31)   | 33(31)    | 160(17)    | 22(20)     |
| 12   | 0(0)       | 0(0)       | 111(22)   | 20(18)    | 48(5)      | 6(6)       |

### 3.4. Examples of Thunderstorms That Produce Large Hailstones

To obtain a conceptual model of the severe hailstorms, some examples have been selected to reproduce the different behaviors. First, it is important to understand the physical meaning of each field. To illustrate this, Figure 8 shows an example of a real case that occurred on the afternoon of 28 July 2022. Images of left panel present the horizontal and vertical sections of a hailstorm that produced severe hail in the region (for instance, in point H in the top-left panel). The right panel contains the zoom to the different used products for the same thunderstorm at the same time (17.24 UTC): Maximum reflectivity (ZMAX), Echo top (45 dBZ, or TOP45), and Vil Density (DVIL), from top to bottom, respectively. Although the structure of the thunderstorm is similar in all three figures, each one has some particularities: the location of the maximum is not the same and there is a high dependance on the vertical development of the storm in the case of TOP45, but also for DVIL. These differences can be explained by the left and bottom middle panels (vertical section across points A to B, and the profiles of the different variables across the line): there are two vertical columns, one more developed at high levels (more close to A point), and the other with very high values of reflectivity at low levels, with lower values at high levels. In this example, ZMAX (black line) is higher for the right structure, while TOP45 (blue line) and DVIL (red line) show the opposite (higher for the left structure).

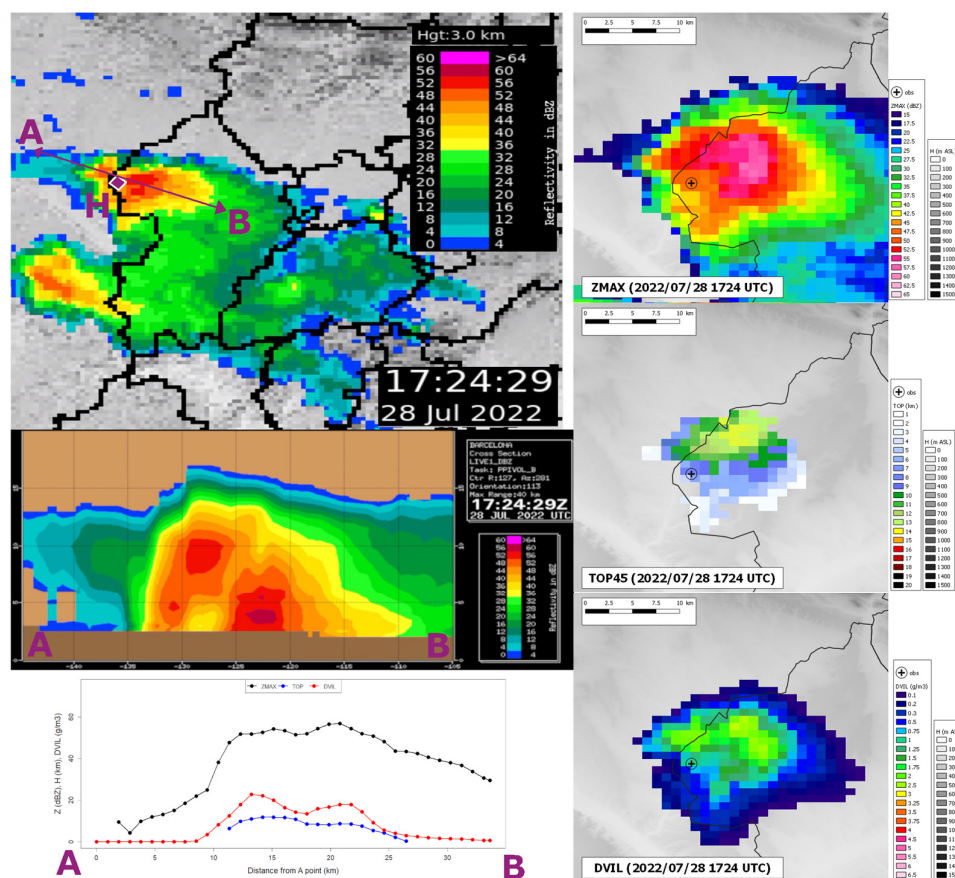


**Figure 8.** The hailfall event of 2022 July 28 at 17.24 UTC. Top left panel shows the CAPPI at 3 km height. H indicates the location of the hail-pad, while A and B are the limits of the segment considered in the vertical section shown in the mid left panel. Bottom left panel shows the radar parameters (ZMAX in black, TOP45 in blue, and DVIL in red) for the same section A-B. Right panels are the fields for the three radar parameters (ZMAX -top-, TOP45 -middle- and DVIL -bottom-).

The evolution of the vertical profile of reflectivity (Figure 9) over the hailfall (“H” point in Figure 8) and the neighborhood 5 km radius (considering the quantiles of 50 -blue-, 90 -red- and 99-black.) allows to understand how the thunderstorm evolved between the 12 minutes prior and the 12 minutes later the event (17.24 UTC). It can be observed how before the hailfall largest reflectivity values (near 50 dBZ) are observed at a height close to 8 km, meanwhile at lowest levels reflectivity is near 20 dBZ. During the approaching of the thunderstorm to the point of observation, reflectivity is rising at all levels, but the maximum is still at high levels. At 17.24 UTC (the estimated time of the hailfall) and the following image, reflectivity curves reach the highest values at all levels, but at 17.30 can be observed how the blue curve is reducing the dimension, mainly at levels between 10 and 15 km. Finally, at 17.36 all the curves are decreasing, indicating that the thunderstorm has finished the hail activity over the observing point.

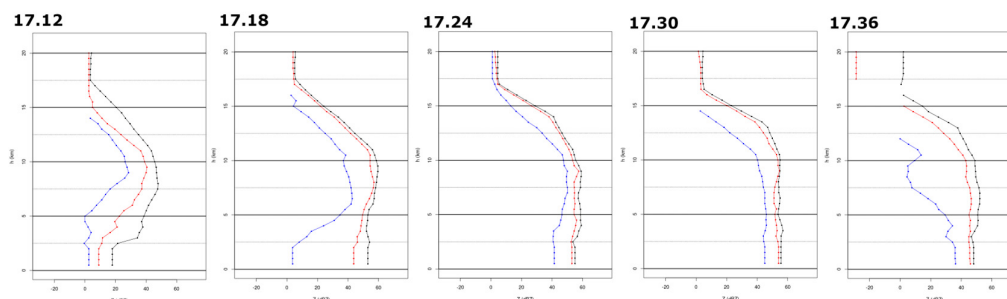


**Figure 9.** Evolution of the Vertical Profiles of Reflectivity (Percentiles of 50 -blue-, 90 -red- and 99 -black-) for the region of 5 km surrounding the hail-pad presented in Figure 8.

As has been cited before, the selected radar variables have a high relationship with the hailstorm structure. To demonstrate this, it is possible to infer the radar variables (ZMAX, TOP45 and DVIL) from these curves, as it is shown in Figure 10. Then, the maximum reflectivity corresponds to the right limit of the black curve, while TOP45 is the Y point when the same curve is crossing the X value of 45. Finally, the VIL density would be equivalent to the area with reflectivity exceeding the 0 dBZ (green area).

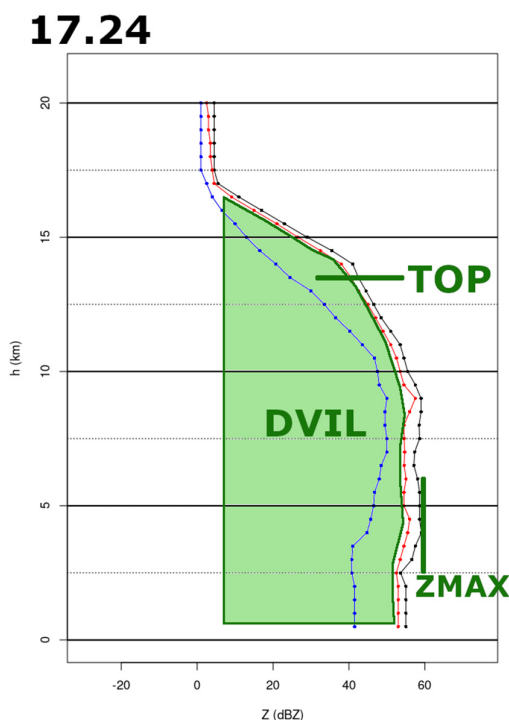


**Figure 10.** Relationship between the Vertical Profiles of Reflectivity with the three radar variables (ZMAX, TOP and DVIL).

Continuing with the differences between both categories, comparing all the curves for the cases with non-severe or severe observations (Figure 11) it is possible to appreciate how the reflectivity values core (the more intense part of the thunderstorm) shows a displacement to the right (higher reflectivity values) in the case of the second category (hailstones with diameter over 2 cm). This difference is still more evident in the case of only considering the time of the hailfall (Figure 12). Therefore, it is more important the shape of the curves than the radar parameter values themselves, because of the limitations that can occur in cases.

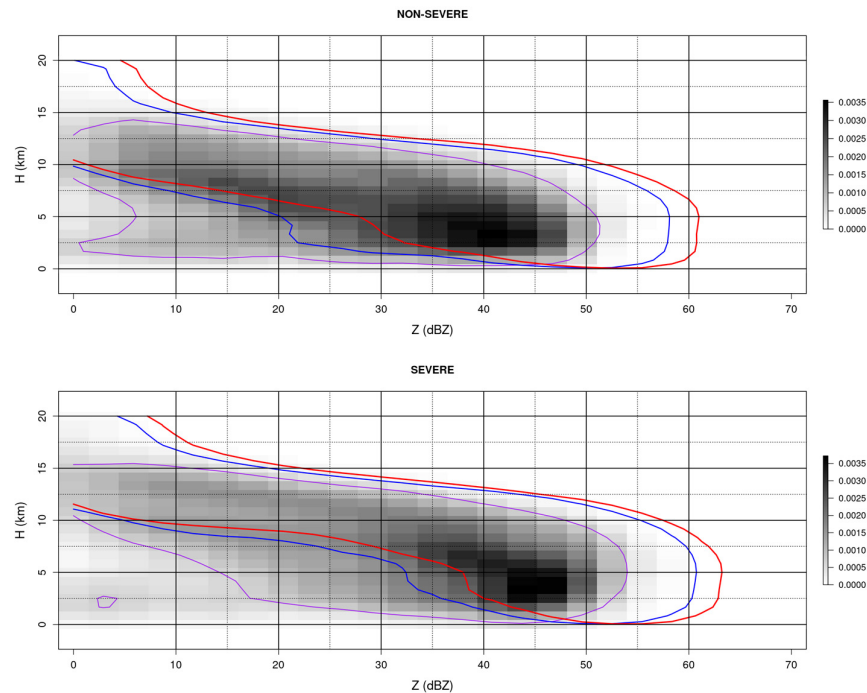


**Figure 11.** Shaded areas show the density of cases for the quantile 50 (surrounded by the purple line) for all the non-severe (top) and severe (below) events of the period 2016-2025, from the Vertical Profiles of Reflectivity. Blue and red lines correspond to the 90 and 99 quantiles.

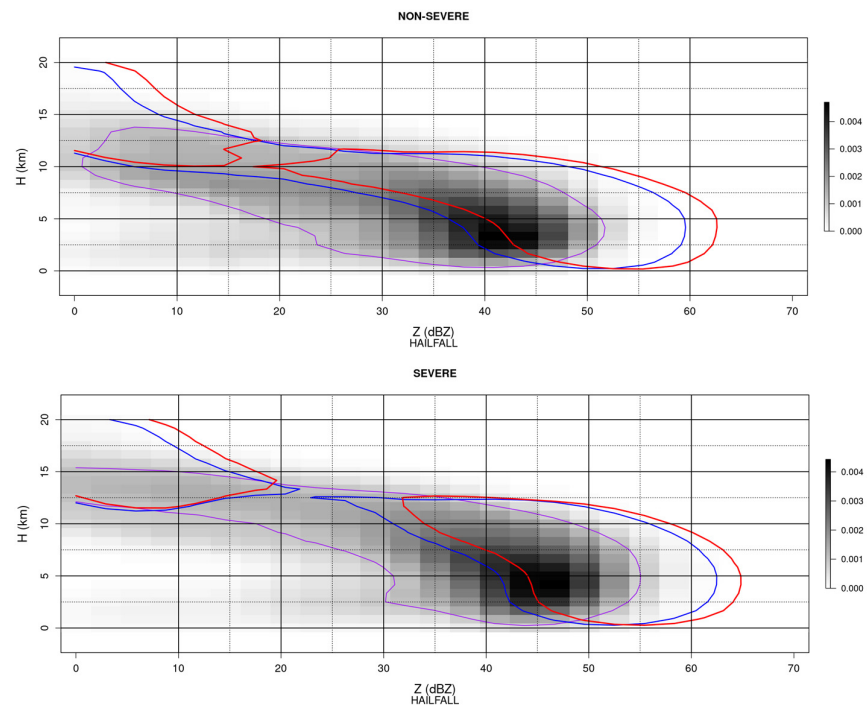


**Figure 12.** Same as Figure 11, but only for the time of the hailfall of each event.

Finally, Figure 13 shows how the life cycle of the hailstorm over those points with non-severe hail (the two top panels) shows for the same period smaller areas of the vertical profile of reflectivity than for those severe hail registers. These differences are more evident during the first three steps (from 12 minutes before the hailstorm to the instant of the event), while for the later images the

differences are not as clear. Therefore, the estimation of the area can provide a signature to discriminate between both types of hail.

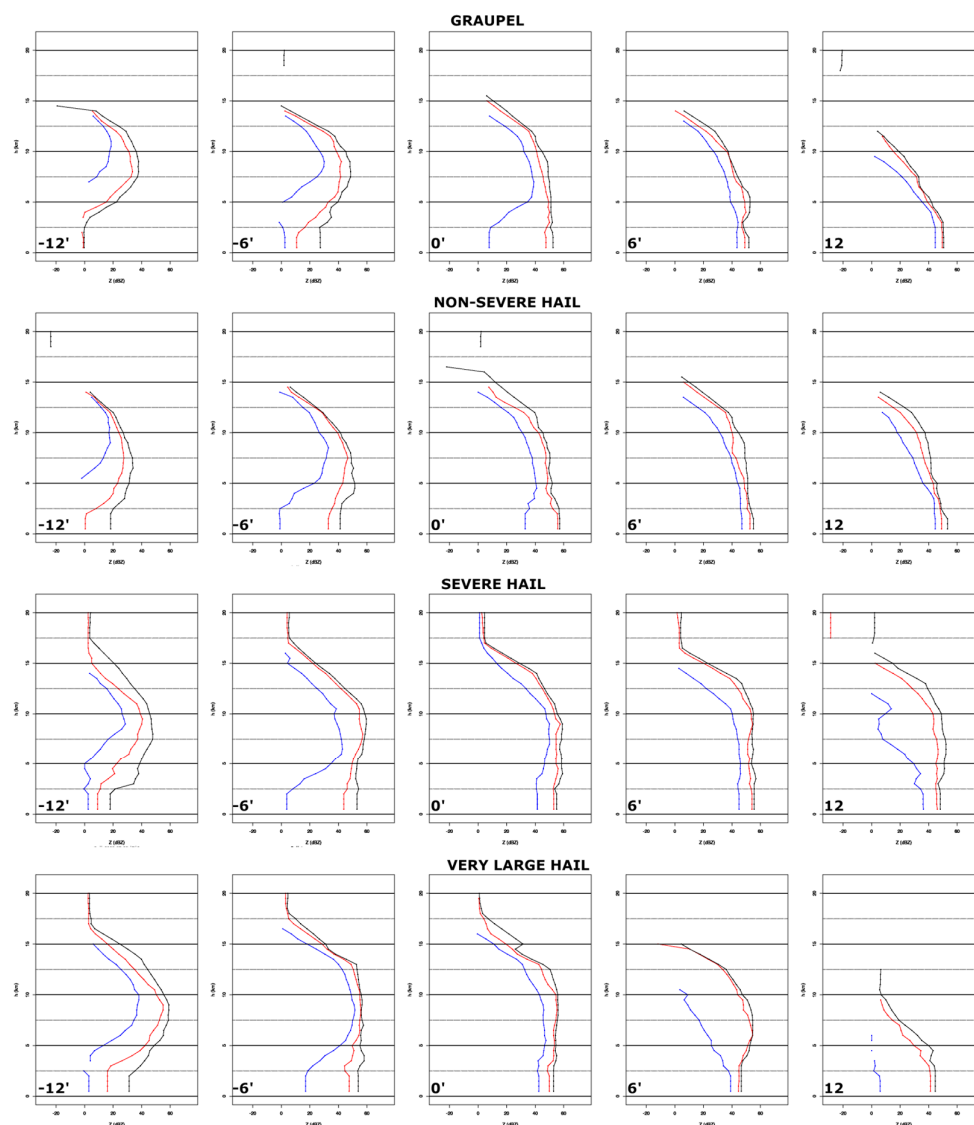


**Figure 13.** Comparison of the Vertical Profiles of Reflectivity for four hail-pads that registered different types of hail during the same event of 2022 July 28.

#### 4. Discussion

The discrimination using weather radar variables between those hailstorms that produce severe or non-severe hail is still a topic of interest. This is because some issues are nowadays still unsolved: problems of radar providing correct values of reflectivity with largest hailstones [1,15,33], the variability of the hail size depending also on internal factors [2,16–19], and the relationship between radar variables and ground registers [3–7]. Most comparisons between radar variables and hail-pad observations [13,15,17,34,35] are made directly. This technique, consisting of searching for a threshold or set of thresholds that fit each possible category, has the previous limitations. Besides, the seasonality of the hail type and size and the changing atmospheric conditions [25,40] implies that similar radar values can provide different ground observations [31,35,36]. As in most of previous studies, the results obtained in the current research indicate that in general largest radar parameters values (on average) are coincident with highest hail size, but there are exceptions.

To reduce the limitation of cases with a miss-identification, this paper focuses on the use of the integration of several vertical profiles of reflectivity around a hail register. The area from the curve of reflectivity exceeding 0 dBZ combines the information from three radar parameters: maximum reflectivity, VIL density and Echo Top. These parameters have been considered in previous research [13,15–17,24,35,36], indicating that none of those and other parameters do not provide individually good results to diagnose large hail in thunderstorms. In fact, some of the previous works assumed that it is necessary to combine some of them.

These curves can be estimated for all the parts of a hailstorm and have provided good results to discriminate different categories of hail in the same event. However, as future research, it is necessary to numerically quantify some thresholds that can help to issue automatic warnings in real time.

## 5. Conclusions

Hailstorms produce large amounts of damage yearly, which has notably increased in the recent years in different regions around the World. Individual products have severe flaws to diagnose different types of hail, even in the same event. Using the combination of hail pads and weather radar variables, this research has focused on using multiple vertical profiles of reflectivity to combine the information of some of those variables (maximum reflectivity, echo top, and VIL density). The combined charts from a ten year period plus a visual analysis of a concrete event with different type of registers showed promising results, with the possibility of implementing in real time to issue surveillance warnings.

**Funding:** This research received no external funding.

**Institutional Review Board Statement:** Not applicable.

**Informed Consent Statement:** Not applicable.

**Data Availability Statement:** The data presented in this study are available on request from the corresponding author due to internal processes applied to the raw data, which are not public available.

**Acknowledgments:** The Author wants to thank to the Servei Meteorologic de Catalunya, ADV-Terres de Ponent and University of Leon for the different types of data provided.

**Conflicts of Interest:** The author declares no conflicts of interest.

## Abbreviations

The following abbreviations are used in this manuscript:

|       |   |
|-------|---|
| ZMAX  | Maximum reflectivity                          |
| DVIL  | VIL Density                                   |
| TOP   | Echo top for a certain reflectivity threshold |
| MESH  | Maximum Expected Size of Hail                 |
| POSH  | Probability of Severe Hail                    |
| SMC   | Servei Meteorologic de Catalunya              |
| VIL   | Vertically Integrated Liquid                  |
| VII   | Vertically Integrated Ice                     |
| HKE   | Hail Kinetic Energy                           |
| POH   | Probability of Hail                           |
| TBSS  | Three-Body Scattering Signature               |
| BWE   | Bounded Weak Echo                             |
| XRAD  | Radar network of the SMC                      |
| CAPPI | Constant Altitude Plan Position Indicator     |

## References

- Allen, J. T.; Giammanco, I. M.; Kumjian, M. R.; Punge, H. J.; Zhang, Q.; Groenemeijer, P.; Kunz, M.; Ortega, K. Understanding hail in the Earth system. *Reviews of Geophysics* **2020**, *58*, e2019RG000665. <https://doi.org/10.1029/2019RG000665>
- Allen, J. T.; Tippett, M. K. The characteristics of United States hail reports: 1955-2014. *E-Journal of Severe Storms Meteorology* **2015**, *10*(3), 1-31. <https://doi.org/10.55599/ejssm.v10i3.60>
- Etkin, D.; Brun, S. E. A note on Canada's hail climatology: 1977-1993. *International Journal of Climatology: A Journal of the Royal Meteorological Society* **1999**, *19*(12), 1357-1373. [https://doi.org/10.1002/\(SICI\)1097-0088\(199910\)19:12<1357::AID-JOC422>3.0.CO;2-B](https://doi.org/10.1002/(SICI)1097-0088(199910)19:12<1357::AID-JOC422>3.0.CO;2-B)
- Mezher, R. N.; Doyle, M.; Barros, V. Climatology of hail in Argentina. *Atmospheric research* **2012**, *114*, 70-82. <https://doi.org/10.1016/j.atmosres.2012.05.020>
- Hulton, F.; Schultz, D. M. Climatology of large hail in Europe: characteristics of the European Severe Weather Database. *Natural Hazards and Earth System Sciences* **2024**, *24*(4), 1079-1098. <https://doi.org/10.5194/nhess-24-1079-2024>
- Li, X.; Zhang, Q.; Zou, T.; Lin, J.; Kong, H.; Ren, Z. Climatology of hail frequency and size in China, 1980-2015. *Journal of Applied Meteorology and Climatology* **2018**, *57*(4), 875-887. <https://doi.org/10.1175/JAMC-D-17-0208.1>
- Raupach, T. H.; Soderholm, J. S.; Warren, R. A.; Sherwood, S. C. Changes in hail hazard across Australia: 1979-2021. *npj Climate and Atmospheric Science* **2023**, *6*(1), 143. <https://doi.org/10.1038/s41612-023-00454-8>
- Prein, A. F.; Holland, G. J. Global estimates of damaging hail hazard. *Weather and Climate Extremes* **2018**, *22*, 10-23. <https://doi.org/10.1016/j.wace.2018.10.004>
- Púčik, T.; Castellano, C.; Groenemeijer, P.; Kühne, T.; Rädler, A. T.; Antonescu, B.; Faust, E. Large hail incidence and its economic and societal impacts across Europe. *Monthly Weather Review* **2019**, *147*(11), 3901-3916. <https://doi.org/10.1175/MWR-D-19-0204.1>
- Palencia, C.; Berthet, C.; Massot, M.; Castro, A.; Dessens, J.; Fraile, R. On the individual calibration of hailpads. *Atmospheric research* **2007**, *83*(2-4), 493-504. <https://doi.org/10.1016/j.atmosres.2006.04.002>
- Battaglia, M.; Lee, C.; Thomason, W.; Fike, J.; Sadeghpour, A. Hail damage impacts on corn productivity: A review. *Crop Science* **2019**, *59*(1), 1-14. <https://doi.org/10.2135/cropsci2018.04.0285>
- Farnell, C.; Batalla, E.; Rigo, T.; Pineda, N.; Sole, X.; Mercader, J.; Martin-Vide, J. Reanalysis of giant hail event in Catalonia (NE of the Iberian Peninsula). *Atmospheric Research* **2023**, *296*, 107051. <https://doi.org/10.1016/j.atmosres.2023.107051>
- Rigo, T.; Llasat, M. C. Forecasting hailfall using parameters for convective cells identified by radar. *Atmospheric research* **2016**, *169*, 366-376. <https://doi.org/10.1016/j.atmosres.2015.10.021>
- Klaus, V.; Krause, J. Investigating hailstorm updrafts and nowcasting hail size using a novel radar-based updraft detection. *Weather and Forecasting* **2024**, *39*(12), 1795-1815. <https://doi.org/10.1175/WAF-D-23-0227.1>
- Blair, S.F.; Laflin, J.M.; Cavanaugh, D.E.; Sanders, K.J.; Currens, S.R.; Pullin, J.I.; Cooper, D.T.; Deroche, D.R.; Leighton, J.W.; Fritchie, R.V.; Mezeul II, M.J.; Goudeau, B.T.; Kreller, S.J.; Bosco, J.J.; Kelly, C.M.; Mallinson, H.M. High-Resolution Hail Observations: Implications for NWS Warning Operations. *Weather and Forecasting* **2017**, *32*(3), 1101-1119. <https://doi.org/10.1175/WAF-D-16-0203.1>
- Blair, S. F.; Deroche, D. R.; Boustead, J. M.; Leighton, J. W.; Barjenbruch, B. L.; Gargan, W. P. A radar-based assessment of the detectability of giant hail. *E-Journal of Severe Storms Meteorology* **2011**, *6*(7), 1-30. <https://doi.org/10.55599/ejssm.v6i7.34>
- Ortega, K. L.; Krause, J. M.; Ryzhkov, A. V. Polarimetric radar characteristics of melting hail. Part III: Validation of the algorithm for hail size discrimination. *Journal of Applied Meteorology and Climatology* **2016**, *55*(4), 829-848. <https://doi.org/10.1175/JAMC-D-15-0203.1>
- Kumjian, M. R.; Lombardo, K.; Loeffler, S. The evolution of hail production in simulated supercell storms. *Journal of the Atmospheric Sciences* **2021**, *78*(11), 3417-3440. <https://doi.org/10.1175/JAS-D-21-0034.1>
- Jayarathne, E. R.; Saunders, C. P. R. The interaction of ice crystals with hailstones in wet growth and its possible role in thunderstorm electrification. *Quarterly Journal of the Royal Meteorological Society* **2016**, *142*(697), 1809-1815. <https://doi.org/10.1002/qj.2777>

20. Phillips, V. T.; Khain, A.; Benmoshe, N.; Ilotoviz, E. Theory of time-dependent freezing. Part I: Description of scheme for wet growth of hail. *Journal of the Atmospheric Sciences* **2014**, *71*(12), 4527-4557. <https://doi.org/10.1175/JAS-D-13-0375.1>
21. Ziegler, C. L.; Ray, P. S.; Knight, N. C. Hail growth in an Oklahoma multicell storm. *Journal of Atmospheric Sciences* **1983**, *40*(7), 1768-1791. [https://doi.org/10.1175/1520-0469\(1983\)040<1768:HGAOM>2.0.CO;2](https://doi.org/10.1175/1520-0469(1983)040<1768:HGAOM>2.0.CO;2)
22. Farnell Barqué, C.; Rigo, T.; Martin-Vide, J.; Úbeda, X. Internal structure of giant hail in a catastrophic event in Catalonia (NE Iberian Peninsula). *Frontiers in Environmental Science* **2024**, *12*, 1479824. <https://doi.org/10.3389/fenvs.2024.1479824>
23. Farley, R. D. Numerical modeling of hailstorms and hailstone growth. Part II: The role of low-density riming growth in hail production. *Journal of Applied Meteorology and Climatology* **1987**, *26*(2), 234-254. [https://doi.org/10.1175/1520-0450\(1987\)026<0234:NMOHAH>2.0.CO;2](https://doi.org/10.1175/1520-0450(1987)026<0234:NMOHAH>2.0.CO;2)
24. Manzato, A.; Riva, V.; Tiesi, A.; Miglietta, M. Observational analysis and simulations of a severe hailstorm in northeastern Italy. *Quarterly Journal of the Royal Meteorological Society* **2020**, *146*(732), 3587-3611. <https://doi.org/10.1002/qj.3886>
25. Farnell, C.; Rigo, T.; Martin-Vide, J. Application of cokriging techniques for the estimation of hail size. *Theoretical and applied climatology* **2018**, *131*(1), 133-151. <https://doi.org/10.1007/s00704-016-1937-0>
26. Brown, T. M.; Pogorzelski, W. H.; Giammanco, I. M. Evaluating hail damage using property insurance claims data. *Weather, Climate, and Society* **2015**, *7*(3), 197-210. <https://doi.org/10.1175/WCAS-D-15-0011.1>
27. Fonseca-Cerda, M.d.S.; de Moel, H.; van Ederen, D.; Schmid, T.; Wouters, L.; Aerts, J.C.J.H.; Botzen, W.J.W.; Haer, T. Hailstorm prediction and loss assessment using high-resolution hazard and claims data. *Atmospheric Research* **2026**, *329*, 108501. <https://doi.org/10.1016/j.atmosres.2025.108501>
28. Dieling, C.; Smith, M.; Beruvides, M. Review of impact factors of the velocity of large hailstones for laboratory hail impact testing consideration. *Geosciences* **2020**, *10*(12), 500. <https://doi.org/10.3390/geosciences10120500>
29. Marcos, J. L.; Sánchez, J. L.; Merino, A.; Melcón, P.; Mérida, G.; García-Ortega, E. Spatial and temporal variability of hail falls and estimation of maximum diameter from meteorological variables. *Atmospheric Research* **2021**, *247*, 105142. <https://doi.org/10.1016/j.atmosres.2020.105142>
30. Rigo, T.; Farnell, C. A Comparison between Radar Variables and Hail Pads for a Twenty-Year Period. *Climate* **2024**, *12*(10), 158. <https://doi.org/10.3390/cli12100158>
31. Sánchez, J. L.; Fraile, R.; De La Madrid, J. L.; De La Fuente, M. T.; Rodríguez, P.; Castro, A. Crop damage: The hail size factor. *Journal of Applied Meteorology and Climatology* **1996**, *35*(9), 1535-1541. [https://doi.org/10.1175/1520-0450\(1996\)035<1535:CDTHSF>2.0.CO;2](https://doi.org/10.1175/1520-0450(1996)035<1535:CDTHSF>2.0.CO;2)
32. Sánchez, J. L.; Gil-Robles, B.; Dessens, J.; Martin, E.; Lopez, L.; Marcos, J. L.; Berthet, C.; Fernández, J.T.; García-Ortega, E. Characterization of hailstone size spectra in hailpad networks in France, Spain, and Argentina. *Atmospheric Research* **2009**, *93*(1-3), 641-654. <https://doi.org/10.1016/j.atmosres.2008.09.033>
33. Trapero, L.; Bech, J.; Rigo, T.; Pineda, N.; Forcadell, D. Uncertainty of precipitation estimates in convective events by the Meteorological Service of Catalonia radar network. *Atmospheric Research* **2009**, *93*(1-3), 408-418. <https://doi.org/10.1016/j.atmosres.2009.01.021>
34. Ortega, K.L. Evaluating multi-radar, multi-sensor products for surface hail-fall diagnosis. *Electronic J. Severe Storms Meteor.* **2018**, *13*(1), 1-36. <https://doi.org/10.55599/ejssm.v13i1.69>
35. Cică, R.; Burcea, S.; Bojariu, R. Assessment of severe hailstorms and hail risk using weather radar data. *Meteorological Applications* **2015**, *22*(4), 746-753. <https://doi.org/10.1002/met.1512>
36. Pilorz, W.; Zięba, M.; Szturc, J.; Łupikasza, E. Large hail detection using radar-based VIL calibrated with isotherms from the ERA5 reanalysis. *Atmospheric Research* **2022**, *274*, 106185. <https://doi.org/10.1016/j.atmosres.2022.106185>
37. Ryzhkov, A. V.; Kumjian, M. R.; Ganson, S. M.; Zhang, P. Polarimetric radar characteristics of melting hail. Part II: Practical implications. *Journal of Applied Meteorology and Climatology* **2013**, *52*(12), 2871-2886. <https://doi.org/10.1175/JAMC-D-13-074.1>
38. Rigo, T.; Farnell, C. A Summary of Hail Events during the Summer of 2022 in Catalonia: A Comparison with the Period of 2013–2021. *Remote Sensing* **2023**, *15*(4), 1012. <https://doi.org/10.3390/rs15041012>

39. Aran, M.; Pena, J.; Torà, M. Atmospheric circulation patterns associated with hail events in Lleida (Catalonia). *Atmospheric research* **2011**, *100*(4), 428-438. <https://doi.org/10.1016/j.atmosres.2010.10.029>
40. Farnell, C.; Rigo, T.; Heymsfield, A. Shape of hail and its thermodynamic characteristics related to records in Catalonia. *Atmospheric Research* **2022**, *271*, 106098. <https://doi.org/10.1016/j.atmosres.2022.106098>
41. Aran, M.; Sairouni, A.; Bech, J.; Toda, J.; Rigo, T.; Cunillera, J.; Moré, J. Pilot project for intensive surveillance of hail events in Terres de Ponent (Lleida). *Atmospheric research* **2007**, *83*(2-4), 315-335. <https://doi.org/10.1016/j.atmosres.2005.09.013>
42. Rigo, T.; Farnell Barqué, C. Evaluation of the radar echo tops in Catalonia: Relationship with severe weather. *Remote Sensing* **2022**, *14*(24), 6265. <https://doi.org/10.3390/cli12100158>
43. García-Ortega, E.; Fita, L.; Romero, R.; López, L.; Ramis, C.; Sánchez, J. L. Numerical simulation and sensitivity study of a severe hailstorm in northeast Spain. *Atmospheric Research* **2007**, *83*(2-4), 225-241. <https://doi.org/10.1016/j.atmosres.2005.08.004>
44. Rigo, T.; Farnell, C. Characterisation of thunderstorms with multiple lightning jumps. *Atmosphere* **2022**, *13*(2), 171, <https://doi.org/10.3390/atmos13020171>.
45. Rigo, T.; Farnell, C. Using maximum Vertical Integrated Liquid (VIL) maps for identifying hail-affected areas: An operative application for agricultural purposes. *J. Mediterr. Meteorol. Climatol* **2019**, *16*, 15-24. <https://doi.org/10.3369/tethys.2019.16.02>
46. Rigo, T.; Llasat, M. C. Forecasting hailfall using parameters for convective cells identified by radar. *Atmospheric research* **2016**, *169*, 366-376. <https://doi.org/10.1016/j.atmosres.2015.10.021>

**Disclaimer/Publisher's Note:** The statements, opinions and data contained in all publications are solely those of the individual author(s) and contributor(s) and not of MDPI and/or the editor(s). MDPI and/or the editor(s) disclaim responsibility for any injury to people or property resulting from any ideas, methods, instructions or products referred to in the content.